

EXACTLY SOLVABLE INTERACTING SPIN-ICE VERTEX MODEL

Anderson A. Ferreira and Francisco C. Alcaraz¹¹Instituto de Física de São Carlos,
Universidade de São Paulo, CP 369, 13560-970, São Carlos, SP, Brazil
(Dated: April 15, 2024)

A special family of solvable five-vertex model is introduced on a square lattice. In addition to the usual nearest neighbor interactions, the vertices defining the model also interact along one of the diagonals of the lattice. Such family of models includes in a special limit the standard six-vertex model. The exact solution of these models gives the first application of the matrix product ansatz introduced recently and applied successfully in the solution of quantum chains. The phase diagram and the free energy of the models are calculated in the thermodynamic limit. The models exhibit massless phases and our analytical and numerical analysis indicate that such phases are governed by a conformal field theory with central charge $c = 1$ and continuously varying critical exponents.

PACS numbers: PACS number(s): 05.50.+q, 47.27.ab, 05.70.-a
Keywords:

I. INTRODUCTION

The six-vertex model was introduced by Pauling in order to explain the residual entropy of ice at zero temperature. Due to its exact integrability and its connection with the XXZ quantum chain, this vertex model is considered as a paradigm of exact integrability [1, 2, 3]. In this model the interactions are between nearest neighbor vertices and are ruled by the geometrical connectivity of the allowed vertex configurations on the lattice. The interaction energy among two vertices is zero for allowed configurations and infinite otherwise. In this paper we introduce a special family of five-vertex models. Besides the usual nearest-neighbor interactions, imposed by their connectivity, there exist additional interactions among vertices at larger distances. Moreover we are going to show that this family of models is exactly integrable and contains as a special case the standard six-vertex model.

Although the introduction of a new exactly integrable model is interesting by itself we would like to mention that recently the interest on two-dimensional vertex models was rised by their possible physical realizations [4]. Artificially produced materials have exhibited a frustrated square-lattice array of nanosize ferromagnetic domains. These materials, for large lattice spacing, are in an ordered "spin-ice" square lattice where their bonds satisfy the six vertex connectivity rules. By decreasing the lattice spacing, the increased frustration produces extra interactions among the vertices as well as other vertex configurations [4].

The solution of the models presented on this paper are obtained through the exact diagonalization of the diagonal-to-diagonal transfer matrix. The exact solution of transfer matrices associated to vertex models or quantum Hamiltonians are usually obtained through the Bethe ansatz [5] on its several formulations. That ansatz asserts that the amplitudes of the eigenfunctions of these operators are given by a sum of appropriate plane waves.

Instead of making use of the Bethe ansatz, the solution we derive will be obtained through the matrix product ansatz recently introduced in [6]. According to this ansatz, the amplitudes of the eigenfunctions are given in terms of a matrix product whose matrices obey special algebraic relations. The present paper presents the first application of the matrix product ansatz for the exact solution of a transfer matrix.

The layout of this papers is as follows. In Sections II and III we introduce the solvable family of interacting vertex models and their associated diagonal-to-diagonal transfer matrix. In Sec. IV we present the matrix product ansatz and diagonalize the transfer matrix obtained in the previous section. Section V presents the general picture of the roots of the spectral parameter equations associated to the exact solution of the models. The free energy in the thermodynamic limit is obtained in Sec. VI whilst in Sec. VII the operator content of the model on its massless phase is obtained by exploring the conformal invariance of the infinite system. Finally in Sec. VIII we conclude our paper with a general discussion.

II. THE INTERACTING FIVE-VERTEX MODEL

The family of vertex models we introduce and solve are defined on a square lattice with M rows and L columns (see Fig. 1a). At each horizontal (vertical) link we attach an arrow pointing to the left or right (up or down) direction. Such arrow configurations can be equivalently described by the vertex configurations of the lattice. A vertex configuration at a given site (center) is formed by the four arrows attached to its links. Similar to the six-vertex model we impose that the allowed arrow configurations only contain vertices satisfying the ice rules, namely, the fugacity of a given vertex is infinite unless two of its four arrows point inward and the two other

ers point outward of its center. In Fig. 2 we show the six vertex configurations respecting the ice rules, with their respective fugacities $c_1; c_2; b_1; b_2; a_0; a_1$. The partition function is given by the sum of all possible vertex configurations with the Boltzmann weights given by the product of the fugacities of the vertices. It is important to notice that the ice rules imply the existence of interactions among the nearest-neighbor vertices. These interactions have a zero or infinite value. For example (see Fig. 2), the vertex with fugacity a_0 has an infinite interaction energy if the vertex on its right side is one of the vertices $(a_1; b_1; c_2)$ or the vertex on its left side is one of the vertices $(a_1; b_1; c_1)$. The model with no extra interactions, besides those given by the connectivity of the vertices on the lattice, is the well known six-vertex model. This model is exactly integrable for arbitrary values of the fugacities, and is considered a prototype of an exact integrable model [1, 2, 3].

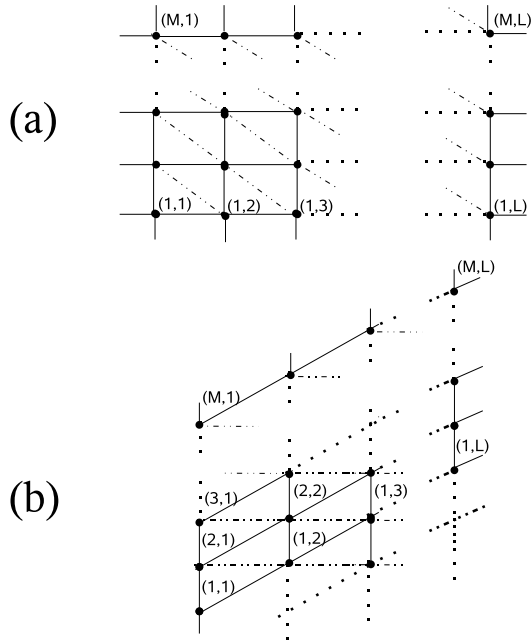


FIG. 1: (a) Square lattice with M horizontal (L vertical) lines. The interacting vertex models have extra interactions along the dashed diagonals. (b) The deformed lattice. The dashed diagonals are now in the horizontal direction.

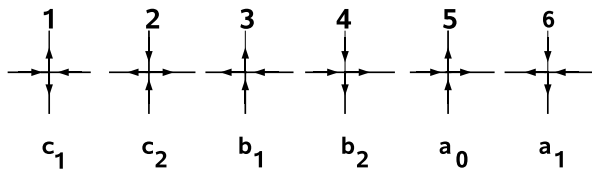


FIG. 2: The six vertex configurations allowed by the ice rules, with their respective fugacities.

We consider a special family of interacting vertex models. Besides the previously mentioned nearest-neighbor interactions (infinite or zero) imposed by the lattice connectivity, the models also contain interactions among pairs of vertices at larger distances. The allowed vertex configurations, with their respective configurations are the first vertex configurations shown in Fig. 2. Contrary to the six-vertex model the vertex configurations with fugacity a_1 are forbidden (zero fugacity).

Such interacting vertex models are labelled by a fixed positive integer t that may take the values $t = 1; 2; 3; \dots$. This parameter specifies the additional interactions among the vertices. These interactions occur along the diagonals of the square lattice that go from the top left to the bottom right direction (see the dashed diagonals in Fig. 1a). A pair of vertices at distance $D = l^2$ ($l = 1; 2; \dots$), in units of lattice spacing, along this diagonal interacts as follows

- a) the interaction energy is zero if $l > t$,
- b) if one of the vertices is a_0 the interaction energy is zero for all values of l ,
- c) if neither of the vertices is a_0 , the interaction energy is infinite if $l \leq t$, except in the special case where $l = t$ and c_2 is on the left of c_1 . In this case the interaction energy e_l is finite and produces a Boltzmann weight φ given by [7]

$$c_l = e^{-e_l} = \frac{a_1}{c_1 c_2} \quad (1)$$

In Fig. 3a and Fig. 3b we show, for the model with $t = 2$, some examples of forbidden (infinite energy) and allowed configurations, respectively. We also show, in those figures, the total contribution of the pair of vertices to the Boltzmann factor. In general, the contribution of a given pair of vertices is zero if the pair is not allowed (infinite interaction energy) or is given by the product of their fugacities (zero interaction energy). The exception to this rule happens when we have the vertices c_1 and c_2 at the distance $D = l^2$ along the diagonal, with c_2 on the left of c_1 (see Fig. 3b). In this case, from (1), the contribution is given by $c_1 c_2 c_l = a_1$.

The partition function of the vertex models are usually calculated by the diagonalization of the row-to-row transfer matrix, connecting the arrow configurations of two consecutive horizontal lines. In the case under consideration, due to the existence of the extra interactions along the diagonals, the calculation is much simpler if we consider the diagonal-to-diagonal transfer matrix, connecting the arrow configurations of two consecutive diagonals of the lattice.

III. THE DIAGONAL-TO-DIAGONAL TRANSFER MATRIX

Following Bariev [8] in order to construct the diagonal-to-diagonal transfer matrix for the interacting vertex

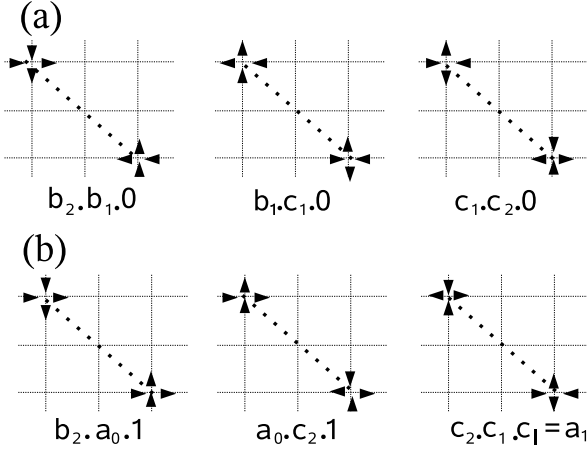


FIG. 3: Examples of forbidden (a) and allowed (b) configurations of pairs of vertices for the interacting vertex model with $t = 2$. The contribution of the vertices to the Boltzmann weights are also shown.

models it is convenient to distort the square lattice shown in Fig. 1a as in Fig. 1b. In this case the vertices which are at closest distances along the dashed diagonals of Fig. 1a are now at the closest distance along the horizontal direction. We are going to solve the model with toroidal boundary conditions on the distorted lattice of Fig. 1b. In the undeformed lattice of Fig. 1a this boundary condition translates into a helical one where we identify the sites

$$(ij) \quad (i+M; j) \quad (i-L; j+L); \quad (2)$$

where $(i; j)$ denote the sites located at the columns j ($j = 1; 2; \dots; L$) and rows i ($i = 1; 2; \dots; M$).

In the distorted lattice of Fig. 1b the allowed vertex configurations of Fig. 2 are shown in Fig. 4. We also represent on this last figure a convenient vertex representation where we only draw the arrow pointing to the down direction. Hereafter we are going to use such representation. We see from Fig. 4 that the allowed vertex configurations have 0 or 2 arrows. We describe a given configuration $\vec{j} >$ of n arrows on a horizontal line of the lattice of Fig. 1b by given their coordinates $(x_1; \dots; x_n)$ and a set of labels $(i_1; \dots; i_n)$, where $i_i = 1$ or $i_i = 2$ depending if we have at the coordinates x_i a vertical or inclined arrow respectively, i. e.,

$$\vec{j} > = \vec{j}_1; i_1; x_2; i_2; \dots; x_n; i_n > ; \quad (3)$$

The diagonal-to-diagonal transfer matrix $T_{D \rightarrow D}$, represented pictorially in Fig. 5, connects the arrow configurations of two horizontal lines in Fig. 1b. Its matrix elements give the contribution of these configurations to the Boltzmann weight. For the allowed configurations they are given by

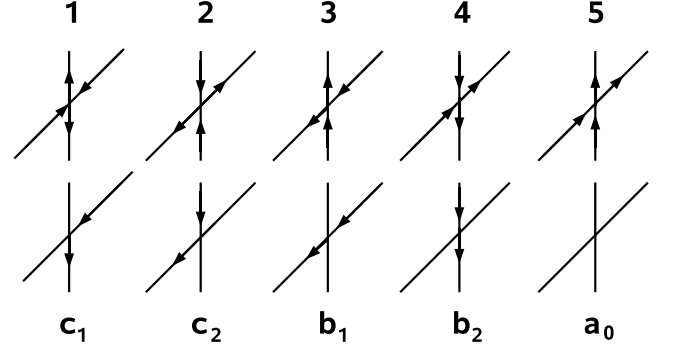


FIG. 4: The allowed vertex configurations in the distorted diagonal lattice with their respective fugacities. In the second line we give a representation where it is only drawn the arrow pointing down.

$$\langle \vec{j} | T_{D \rightarrow D} | \vec{j}^0 \rangle = c_1^{n_1} c_2^{n_2} b_1^{n_3} b_2^{n_4} a_0^{n_5} c_1^{n_p}; \quad (4)$$

where n_i are the number of vertices of type i ($i = 1; \dots; 5$) and n_p is the number of pairs of vertices $c_2 \ c_1$ at distance of t units along the horizontal lines (see Fig. 5). The partition function is given by the trace

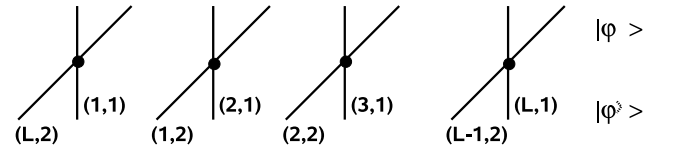


FIG. 5: Pictorial representation of the diagonal-to-diagonal transfer matrix. The coordinates $(i; j)$ specify the possible arrows positions.

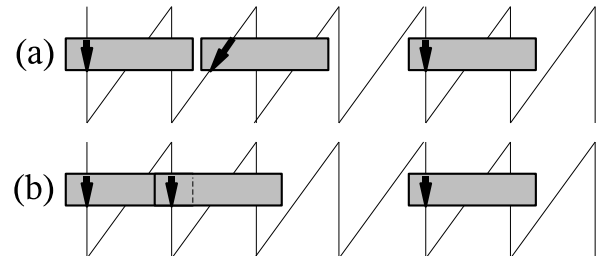


FIG. 6: Example of an allowed (a) and not allowed (b) configuration of the interacting vertex model with $t = 1$. The arrows have an effective hard-core size $s = 2t + 1 = 3$.

$$Z = \text{Tr}(T_{D-D}^M) : \quad (5)$$

It is interesting to observe that in the distorted lattice the allowed arrow configurations on the horizontal lines, besides having a fixed number of arrows, could also be interpreted as if the arrows would have an effective size $s = 2t + 1$ ($s = 3; 5; \dots$), in lattice spacing units of the distorted lattice. An arrow on a given link has hard-core interactions that exclude the occupation of other arrows at the link itself as well as at the $2t$ -nearest links on its right. In Fig. 6 we represent pictorially an allowed (a) and a not allowed (b) configuration of arrows for the interacting vertex model with $t = 1$. This example corresponds to arrows of effective size $s = 3$.

The above interpretation, where we associate an effective size to the arrows, allows us a simple extension of our model to the case where $t = 0$. In this case the arrows have a unity size and the extra hard-core interactions among the vertices with fugacities c_2 and c_1 occur when the arrows are at the same site, thus giving rise to an extra vertex with fugacity $c_1 c_2 \frac{a_1}{c_1 c_2} = a_1$, and hence the model reduces to the well known six-vertex model, with fugacities given in Fig. 2.

IV. THE MATRIX PRODUCT ANSATZ AND THE DIAGONALIZATION OF THE TRANSFER MATRIX T_{D-D}

In this section we solve the eigenvalue equation for the diagonal-to-diagonal transfer matrix T_{D-D} introduced in the previous section. As a consequence of the arrow conservation and the translation invariance of the arrow configurations on the horizontal lines of Fig. 1b the matrix T_{D-D} can be splitted into block disjoint sectors labelled by the number n ($n = 0; 1; \dots; 2L$) of arrows and momentum $p = \frac{2}{L}j$ ($j = 0; 1; \dots; L-1$). We want to solve, in each of these sectors, the eigenvalue equation

$$T_{D-D} j_{n,p} > = \lambda j_{n,p} > ; \quad (6)$$

where $j_{n,p} >$ and λ are the eigenvalues and eigenvectors of T_{D-D} , respectively. These eigenvectors can be written in general as

$$\begin{aligned} j_{n,p} > &= \sum_{x_1, \dots, x_n} P_{1, \dots, n}(x_1; \dots; x_n) |x_1; \dots; x_n; n >; \\ &\text{fix } f, g \end{aligned} \quad (7)$$

where $P_{1, \dots, n}(x_1; \dots; x_n)$ is the amplitude corresponding to the arrow configuration where n arrows of type $(1; \dots; n)$ are located at $(x_1; \dots; x_n)$, respectively. The symbol $(*)$ in (7) means that the sums of f, g and

g are restricted to the sets obeying the hard-core exclusions, for a given interacting parameter t :

$$x_{i+1} \neq x_i + t + 1, \quad i; 1 \neq i+1; 2; \quad (8)$$

for $i = 1; \dots; n-1$, and

$$t+1 \neq i; 1 \neq n; 2, \quad x_n \neq x_1 - L, \quad t+1 \neq n; 1 \neq i; 2 : \quad (9)$$

Since $j_{n,p} >$ is also an eigenvector with momentum p , then the amplitudes satisfy

$$\frac{P_{1, \dots, n}(x_1; \dots; x_n)}{P_{1, \dots, n}(x_1 + 1; \dots; x_n + 1)} = e^{ip}; \quad (10)$$

for $x_n = L-1$, whilst for $x_n = L$

$$\frac{P_{1, \dots, n}(x_1; \dots; L)}{P_{1, \dots, n}(1; x_1 + 1; \dots; x_{n-1} + 1)} = e^{ip} : \quad (11)$$

The exact solution of (6) is obtained by an appropriate ansatz for the unknown amplitudes $P_{1, \dots, n}(x_1; \dots; x_n)$. As shown in the last section our model reduces to the standard six-vertex model for the case where $t = 0$ ($s = 1$). An appropriate coordinate Bethe ansatz, that solves the eigenvalue equation (6), is known in this case [9]. Thus the amplitudes $P_{1, \dots, n}(x_1; \dots; x_n)$ are given, as usual, by a combination of plane waves whose wavenumbers are fixed by the eigenvalue equation (6).

In this paper we solve (6), for general values of t ($t = 0; 1; 2; \dots$) or $s = 2t + 1$ ($s = 1; 3; 5; \dots$), by using a distinct ansatz. The matrix product ansatz we are going to use was introduced in [6] for exact integrable quantum chains. We present in this paper the first application of this matrix product ansatz for transfer matrices. According to such ansatz the amplitudes $P_{1, \dots, n}(x_1; \dots; x_n)$ are given in terms of a matrix product satisfying an unknown associative algebra. The model is exactly integrable if the eigenvalue equations consistently the algebraic relations among the matrices.

In order to formulate the matrix product ansatz we make a one-to-one correspondence between configurations of arrows and products of matrices. The matrix product associated to a given arrow configuration is obtained by associating a matrix E to the sites with no arrow, a matrix $A^{(1)}$ to the sites with a single arrow of type $(1; 2)$, and finally the matrix $A^{(1)} E^{-1} A^{(2)}$ to the sites with two arrows [10]. The unknown amplitudes in (7) are obtained by associating them to the matrix product ansatz

$$P_{1, \dots, n}(x_1; \dots; x_n) = E^{x_1-1} A^{(1)} E^{x_2-x_1-1} A^{(2)} \dots E^{x_n-x_{n-1}-1} A^{(n)} E^{L-x_n} : \quad (12)$$

Actually E and A are abstract operators with an associative product. A well defined eigenfunction is obtained, apart from a normalization factor, if all the amplitudes

are uniquely related. Equivalently, in the subset of words (products of matrices) of the algebra containing n matrices A and $(L - n)$ matrices E , there exists only a single independent word. The relation between any two words gives the ratio between the corresponding amplitudes in (12).

We could also formulate the ansatz (12) by associating a complex number to the single independent word. We can choose any operation for the matrix products that gives a non-zero scalar. In the original formulation of the matrix product ansatz for exactly integrable quantum chains with periodic boundary conditions [6], the trace operation was chosen to produce the following scalar

$$P_{1, \dots, n}(x_1, \dots, x_n) = \text{Tr}[E^{x_1-1} A^{(1)} E^{x_2-x_1-1} A^{(2)} \dots E^{x_n-x_{n-1}-1} A^{(n)} E^{L-x_n-1}]; \quad (13)$$

The matrix P was chosen to have a given algebraic relation with the matrices E and A . Recently, Golinelli and Mallick [11] have shown that in the particular case of the asymmetric exclusion problem in a periodic chain it is possible to formulate the ansatz only by imposing relations between the matrices E and P . The relations between A and P is then totally arbitrary. Actually, as we are going to show in this paper, we do not need to impose any algebraic relation between the matrices E and A with P . The matrix P can be any arbitrary matrix that produces a non-vanishing trace in (13). This observation is not particular to the present model. It is valid for any of the exactly integrable quantum chains solved in the original formulation of the matrix product ansatz [6]. Instead of restricting our matrix product ansatz with the trace operation, as in (13), we will consider the more general formulation given by (12).

Since the eigenfunctions produced by the ansatz have a well-defined momentum $p = \frac{2\pi}{L}j$ ($j = 0, \dots, L-1$), the relations (10) and (11) imply the following constraints for the matrix products appearing in the ansatz (12)

$$E^{x_1-1} A^{(1)} E^{x_2-x_1-1} \dots A^{(n)} E^{L-x_n-1} = e^{ip} E^{x_1} A^{(1)} E^{x_2-x_1-1} \dots A^{(n)} E^{L-x_n-1}; \quad (14)$$

for $x_n = L-1$, and for $x_n = L$

$$E^{x_1-1} A^{(1)} E^{x_2-x_1-1} \dots A^{(n)} = e^{ip} A^{(n)} E^{x_1-1} A^{(1)} \dots A^{(n-1)} E^{L-x_{n-1}-1}; \quad (15)$$

In order to proceed, in the usual way, we are going to consider firstly the eigensectors of T_D with small values of n .

$n = 0$. We have the trivial solution presenting a single eigenvalue $\lambda_0 = a_0^L$.

$n = 1$. We have in this case $2L$ possible configurations, corresponding to a single arrow of type $\sigma = 1, 2$ at any lattice position $x = 1, \dots, L$. The eigenvalue equation (6) gives us the $2L$ equations

$$\frac{1}{a_0^{L-1}} E^{x-1} A^{(1)} E^{L-x} = b_2 E^{x-1} A^{(1)} E^{L-x} + c_1 E^{x-1} A^{(2)} E^{L-x}; \quad (16)$$

for $x = 1, \dots, L$,

$$\frac{1}{a_0^{L-1}} E^{x-1} A^{(2)} E^{L-x} = c_2 E^{x-1} A^{(1)} E^{L-x-1} + b_1 E^{x-1} A^{(2)} E^{L-x-1}; \quad (17)$$

for $x = 1, \dots, L-1$, and for $x = L$

$$\frac{1}{a_0^{L-1}} E^{L-1} A^{(2)} = c_2 A^{(1)} E^{L-1} + b_1 A^{(2)} E^{L-1}; \quad (18)$$

These equations are written in a convenient form by imposing that both matrices $A^{(\sigma)}$ ($\sigma = 1, 2$) depend on a single spectral parameter matrix A_k :

$$A^{(1)} = \frac{1}{2} A_k E^{1-2t}; \quad A^{(2)} = \frac{1}{2} A_k E^{1-2t}; \quad (19)$$

where $\frac{1}{2}$ and $\frac{1}{2}$ are unknown scalars and A_k satisfies the following algebraic relation with the matrix E

$$E A_k = e^{ik} A_k E; \quad (20)$$

Inserting (19) on (16) we obtain

$$\left(\frac{1}{2} \frac{1}{2} \quad b_2 a_0^{L-1} \frac{1}{2} \quad c_1 a_0^{L-1} \frac{1}{2} \right) E^{x-1} A_k E^{1-2t} E^{L-x} = 0; \quad (21)$$

On the other hand inserting (19) on (17)–(18) and using (20) we obtain

$$\left(\frac{1}{2} \frac{1}{2} \quad c_2 a_0^{L-1} \frac{1}{2} e^{ik} \quad b_1 a_0^{L-1} \frac{1}{2} e^{ik} \right) E^{x-1} A_k E^{1-2t} E^{L-x} = 0; \quad (22)$$

for $x = 1, \dots, L-1$ and

$$\left(\frac{1}{2} e^{ikL} \frac{1}{2} \quad c_2 a_0^{L-1} \frac{1}{2} e^{ik} \quad b_1 a_0^{L-1} \frac{1}{2} e^{ik} \right) A_k E^{L-2t} = 0; \quad (23)$$

However by inserting (20) in (14) we verify that k coincide with the momentum of the eigenstate:

$$k = p = \frac{2\pi m}{L}; \quad m = 0, 1, \dots, L-1; \quad (24)$$

In order to produce a non-zero norm state we should impose $E^{x-1} A_k E^{1-2t} E^{L-x} \neq 0$, for $x = 1, \dots, L$. Due

to the equality $e^{ikL} = 1$, equations (21)–(23) reduce to the eigenvalue problem of a 2×2 matrix

$$\frac{1}{a_0^{L/2}} \begin{pmatrix} 1 \\ 1 \end{pmatrix} = \begin{pmatrix} b_2 & c_1 \\ c_2 e^{ik} & b_1 e^{ik} \end{pmatrix} \begin{pmatrix} 1 \\ 1 \end{pmatrix} : \quad (25)$$

The diagonalization of (25) gives us the eigenvalue

$$\begin{aligned} \lambda_1(k) &= \lambda_1^{(1)}(k) = \frac{a_0^{L/2}}{2} (b_2 + b_1 e^{ik} \\ &+ 1[(b_2 + b_1 e^{ik})^2 - 4e^{ik}(b_2 b_1 - c_2 c_1)]^{1/2}); \quad (26) \end{aligned}$$

with $\lambda = \lambda_1$ and k given by (24).

$n = 2$. The eigenvalue equation (6) gives two types of relations for the amplitudes (12). The configuration where we have no collisions, i. e., $k_1; 1; x_2; 2 > 0$, $k_1; 2; x_1 + t + 1; 1 > 0$ gives generalizations of the equations (16)–(18) for two particles

$$\begin{aligned} \frac{2}{a_0^{L/2}} E^{x_1-1} A^{(1)} E^{x_2-x_1-1} A^{(1)} E^{L-x_2} = \\ b_2^2 E^{x_1-1} A^{(1)} E^{x_2-x_1-1} A^{(1)} E^{L-x_2} \\ + c_1 b_2 E^{x_1-1} A^{(2)} E^{x_2-x_1-1} A^{(1)} E^{L-x_2} \\ + b_2 c_1 E^{x_1-1} A^{(1)} E^{x_2-x_1-1} A^{(2)} E^{L-x_2} \\ + c_1^2 E^{x_1-1} A^{(2)} E^{x_2-x_1-1} A^{(2)} E^{L-x_2}; \quad (27) \end{aligned}$$

$$\begin{aligned} \frac{2}{a_0^{L/2}} E^{x_1-1} A^{(2)} E^{x_2-x_1-1} A^{(1)} E^{L-x_2} = \\ c_2 b_2 E^{x_1-1} A^{(1)} E^{x_2-x_1-2} A^{(1)} E^{L-x_2} \\ + b_1 b_2 E^{x_1-1} A^{(2)} E^{x_2-x_1-2} A^{(1)} E^{L-x_2} \\ + c_2 c_1 E^{x_1-1} A^{(1)} E^{x_2-x_1-2} A^{(2)} E^{L-x_2} \\ + b_1 c_1 E^{x_1-1} A^{(2)} E^{x_2-x_1-2} A^{(2)} E^{L-x_2}; \quad (28) \end{aligned}$$

$$\begin{aligned} \frac{2}{a_0^{L/2}} E^{x_1-1} A^{(1)} E^{x_2-x_1-1} A^{(2)} E^{L-x_2} = \\ c_2 b_2 E^{x_1-1} A^{(1)} E^{x_2-x_1-1} A^{(1)} E^{L-x_2-1} \\ + c_1 c_2 E^{x_1-1} A^{(2)} E^{x_2-x_1-1} A^{(1)} E^{L-x_2-1} \\ + b_2 b_1 E^{x_1-1} A^{(1)} E^{x_2-x_1-1} A^{(2)} E^{L-x_2-1} \\ + c_1 b_1 E^{x_1-1} A^{(2)} E^{x_2-x_1-1} A^{(2)} E^{L-x_2-1}; \quad (29) \end{aligned}$$

$$\begin{aligned} \frac{2}{a_0^{L/2}} E^{x_1-1} A^{(2)} E^{x_2-x_1-1} A^{(2)} E^{L-x_2} = \\ c_2^2 E^{x_1-1} A^{(1)} E^{x_2-x_1-1} A^{(1)} E^{L-x_2-1} \\ + b_1 c_2 E^{x_1-1} A^{(2)} E^{x_2-x_1-1} A^{(1)} E^{L-x_2-1} \\ + c_2 b_1 E^{x_1-1} A^{(1)} E^{x_2-x_1-1} A^{(2)} E^{L-x_2-1} \\ + b_1^2 E^{x_1-1} A^{(2)} E^{x_2-x_1-1} A^{(2)} E^{L-x_2-1}; \quad (30) \end{aligned}$$

In the case where $x_2 = L$, equations (29) and (30) are replaced by

$$\begin{aligned} \frac{2}{a_0^{L/2}} E^{x_1-1} A^{(1)} E^{L-x_1-1} A^{(2)} = \\ c_2 b_2 A^{(1)} E^{x_1-2} A^{(1)} E^{L-x_1} \\ + c_1 c_2 A^{(1)} E^{x_1-2} A^{(2)} E^{L-x_1} \\ + b_2 b_1 A^{(2)} E^{x_1-2} A^{(1)} E^{L-x_1} \\ + c_1 b_1 A^{(2)} E^{x_1-2} A^{(2)} E^{L-x_1}; \quad (31) \end{aligned}$$

$$\begin{aligned} \frac{2}{a_0^{L/2}} E^{x_1-1} A^{(2)} E^{L-x_1-1} A^{(2)} = \\ c_2^2 A^{(1)} E^{x_1-1} A^{(1)} E^{L-x_1-1} \\ + b_1 c_2 A^{(1)} E^{x_1-1} A^{(2)} E^{L-x_1-1} \\ + c_2 b_1 A^{(2)} E^{x_1-1} A^{(1)} E^{L-x_1-1} \\ + b_1^2 A^{(2)} E^{x_1-1} A^{(2)} E^{L-x_1-1}; \quad (32) \end{aligned}$$

On the other hand, the configurations $k_1; 2; x_2 = x_1 + t + 1; 1 > 0$, where we have collision of the arrows, give us, instead, the equations

$$\begin{aligned} \frac{2}{a_0^{L/2}} E^{x_1-1} A^{(2)} E^{t-1} A^{(1)} E^{L-x_1-t-1} = \\ a_1 E^{x_1-1} A^{(1)} E^{t-1} A^{(2)} E^{L-x_1-t-1}; \quad (33) \end{aligned}$$

where we have used the interaction energy $e_t = \frac{a_1}{c_1 c_2}$, given by (1). As in the case $n = 1$ we identify the matrices $A^{(i)} (i = 1; 2)$ as composed by two spectral dependent matrices A_{k_1} and A_{k_2} :

$$A^{(i)} = \sum_{i=1}^2 X^i A_{k_i} E^{1-2t}; \quad (34)$$

where $X^i (i = 1; 2)$ are unknown scalars and the spectral dependent matrices obey the commutation relation with the matrix E

$$E A_{k_j} = e^{ik_j} A_{k_j} E; \quad j = 1; 2; \quad (35)$$

The relations (34) and (35), when inserted in (14) with $n = 2$, relate the momentum of the eigenstate with the spectral parameters:

$$p = k_1 + k_2; \quad (36)$$

Using (34)–(36) in (27)–(32) the non-zero norm condition for the eigenstate gives, for any x_1 and x_2 , a single set of equations for the scalars $X^i (i = 1; 2)$:

$$A_{k_j} A_{k_1} = s(k_j; k_1) A_{k_1} A_{k_j}; \quad A_{k_j}^2 = 0; \quad j = 1; \dots; n; \quad (51)$$

where $s(k_j; k_1)$ is given by (45). The equations with more than two arrows at collisions give relations that are automatically satisfied, due to the associativity of the algebra of the matrices A_{k_j} ($j = 1; \dots; n$). The eigenvalues of the transfer matrix are given by

$$\lambda_n(k_1; \dots; k_n) = \prod_{j=1}^n \lambda_1(k_j); \quad (52)$$

The spectral parameters k_j are fixed by the boundary relation (15) and are given by the solution of the nonlinear set of equations

$$e^{ik_j L} = \prod_{l=1}^n s(k_j; k_l) \frac{e^{ik_j} e^{2it}}{e^{ik_1}}; \quad j = 1; \dots; n; \quad (53)$$

with $s(k_j; k_l)$ given by (45). This last equation reproduces for $t = 0$ the spectral parameter equations for the six-vertex model obtained in [9] by using the coordinate Bethe ansatz.

Since $p = \sum_{j=1}^n k_j$ we can rewrite the spectral parameter equations (53), in the sector with a number n ($n = 1; 2; \dots$) of arrows and momentum $p = \frac{2-j}{L}$ ($j = 0; 1; \dots; L-1$), as

$$e^{ik_j(L-2nt)} e^{2ipt} = \prod_{l=1}^n s(k_j; k_l); \quad (54)$$

Consequently the eigenvalues belonging to the sector labelled by $(n; p)$ of T_{D-D} of the interacting vertex model with a parameter t ($t = 0; 1; 2; \dots$) are related to those of the standard six-vertex model ($t = 0$). The six-vertex model is defined on a lattice size $L^0 = L - 2nt$ and with a momentum dependent seam [13] along the vertical direction of Fig. 1b. The same phenomenon also happens on quantum Hamiltonians with hard-core exclusion effects [12].

We should mention that it is also possible to reobtain our solution of the interacting vertex models by using the coordinate Bethe ansatz. The eigenfunctions we derived through the matrix product ansatz give the educated guess that we should use for the coordinate Bethe ansatz. The spectral parameter equations we obtain are the same as (53).

Before closing this section let us give a possible representation for the matrices A and E of the ansatz (12). For a given solution $f(k_1; \dots; k_n)$ of the spectral parameter equations (54), in the sector with n particles, the matrices E and $f A_{k_1}; \dots; A_{k_n}$ have the following finite-dimensional representation

$$E = \prod_{l=1}^n \begin{pmatrix} 1 & 0 \\ 0 & e^{ik_l} \end{pmatrix};$$

$$A_{k_j} = \begin{matrix} \text{"} & \text{"} & \text{"} & \text{"} \\ \begin{matrix} \emptyset & 1 \\ 1 & 1 \end{matrix} & s(k_j; k_1) & \begin{matrix} 0 & 0 \\ 0 & 1 \end{matrix} & \begin{matrix} 0 & 1 \\ 0 & 0 \end{matrix} \\ \text{"} & \text{"} & \text{"} & \text{"} \\ \begin{matrix} 1 & 0 \\ 0 & 1 \end{matrix} & & & \end{matrix}; \quad (55)$$

where $s(k_j; k_1)$ are given by (45) and A is obtained from (48). The dimension of the representation is 2^n and the products appearing on the ansatz are traceless. If we want a formulation of the matrix product ansatz where the trace operation is used, as in the formulation (13), it is quite simple to produce the matrix p that gives a non-zero value for the trace. We should stress that in the original formulation of the ansatz [6], it was required unnecessary additional algebraic relations of the matrices E and A with the boundary matrix p . The representations, in this case, are probably in finite dimensional.

V. ROOTS OF THE SPECTRAL PARAMETER EQUATIONS

In order to complete the solution of any integrable model we need to find the roots of the associated spectral parameter equations (Eq. (53) in our case). The solution of those equations is in general a quite difficult problem for finite L . However numerical analysis on small lattices allows us to conjecture, for each problem, the particular distributions of roots that correspond to the most important eigenvalues in the bulk limit ($L \rightarrow \infty$). Those are the eigenvalues with larger real part in the case of transfer matrix calculations. The equations we obtained in the last section were never analyzed previously either for finite or in finite values of L . Even in the simplest case $t = 0$, where the model reduces to the six-vertex model, the spectral parameter equations obtained in [9], through the Bethe ansatz, were not analyzed in the literature. A detailed numerical analysis of the Bethe ansatz equations for the row-to-row transfer matrix of the six-vertex model, or the XXZ chain was previously done [14, 18]. However, as we saw in last section, the corresponding equations for the diagonal-to-diagonal transfer matrix of the six-vertex model are quite different and a numerical study of these equations is still missing.

In our general solution of last section we have, for arbitrary values of the interacting range t ($t = 0; 1; 2; \dots$), two free parameters: $(a; b; c; d)$. The particular case where we have no interactions along the diagonals ($a_1 = 0$) is special and is not going to be considered here (see [15] for a discussion of the parameterization in this case).

In order to simplify our analysis we are going hereafter to restrict ourselves to a symmetric version of our model with only three free parameters $(a; b; c)$, namely,

$$a_0 = 1; \quad a_1 = a^2; \quad b_1 = b_2 = b; \quad c_1 = c_2 = c; \quad (56)$$

The parameter t gives, in the case where $t = 0$, the contribution to the fugacity due to an electric field on the symmetric six-vertex model. For general values of t , $t = e^{\ln t}$, plays the role of a chemical potential controlling the number of arrows in the thermodynamic limit.

Instead of writing the spectral parameter equations in terms of the spectral parameters $(k_1; \dots; k_n)$ as in (54), it is more convenient to write these equations in terms of the variables $f_j = \frac{1}{2} \ln(k_j)$, with k_j given by (26). In this case the eigenvalues of T_{D-D} are given by

$$\lambda_n = \lambda_{n-1} \lambda_{n+1}; \quad (57)$$

where f_j satisfy

$$\frac{b(f_j - f_{j-1})}{b(f_j - f_{j+1})} \frac{c^{L-2n}}{c^2} e^{2ipt} = \prod_{l=1}^n \frac{1 - f_j - 2}{1 - f_j - 2} \frac{j+1}{j+1}; \quad j = 1; \dots; n; \quad (58)$$

and we have introduced the anisotropy parameter

$$= \frac{b^2 - c^2 + 1}{2b}; \quad (59)$$

We see, from (57)-(59), that we have now only two free parameters: b and c . The interacting parameter t , that gives the contribution due to the interactions among the vertices along the diagonal, does not appear on the equations (58) and (59). It only gives an overall scale for the eigenvalues as shown in (57). Inspired on the usual parameterization of the six-vertex model [2] we express the parameters b and c in terms of the parameters α and β :

$$b = b(\alpha; \beta) = \frac{\sin \alpha}{\sin(\alpha - \beta)}; \quad c = c(\alpha; \beta) = \frac{\sin \beta}{\sin(\alpha - \beta)}; \\ = \cos \beta; \quad (60)$$

The fact that α is a real number implies that α is real for $1 \leq j \leq n$, and pure imaginary for $j > n$. Since the right-hand side of (58) is the same for all values of the parameter t it is interesting, as in the six-vertex model [9], to make the change of variables $f_j \rightarrow f_j$, where,

$$f_j = \frac{\sinh(i\alpha_j)}{\sinh \beta}; \quad j = 1; \dots; n; \quad (61)$$

In terms of these new variables f_j the spectral parameter equations (58) become

$$\frac{\sinh(i\alpha_j - i\alpha_{j-1}) \sinh(i\alpha_j - i\alpha_{j+1})}{\sinh(\beta - i\alpha_j) \sinh(\beta + i\alpha_j)} \frac{c^{L-2n}}{c^2} e^{2ipt} = \prod_{l=1}^n \frac{\sinh(\beta - i\alpha_{j-1} - i\alpha_j)}{\sinh(\beta - i\alpha_j - i\alpha_{j+1})}; \quad j = 1; \dots; n; \quad (62)$$

These equations are quite distinct from the corresponding spectral parameter equations derived for the row-to-row transfer matrix of the six-vertex model [1, 2]. Since no numerical analysis of the roots for this type of equations were reported in the literature, we made an extensive numerical study of them for finite values of L and several values of the anisotropy β . In the particular case where $\beta = 0$ ($\alpha = \frac{\pi}{2}$) these equations can be solved analytically. Solutions of these equations are obtained by the Newton method by using the distribution of roots f_j at $\beta = 0$ as the starting point to obtain the corresponding roots at other values of $\beta \neq 0$. Our numerical analysis shows that the eigenspectrum of T_{D-D} is formed by real or complex-conjugated pairs of roots ensuring that the partition function (5) is a real number. We verified that the eigenvalue with highest real part, belonging to the sector with n arrows, is real and corresponds to a zero momentum eigenstate ($p = 0$). The distribution of roots f_j corresponding to this eigenvalue has a fixed imaginary part, that depends on α and β , and a symmetrically distributed real part, i.e.,

$$\text{Im}(f_j) = \frac{\alpha - \beta}{2}; \quad \text{Real}(f_j) = \text{Real}(f_{n-j+1}); \\ j = 1; \dots; n; \quad (63)$$

We have also verified, for all sectors, the occurrence of several other real eigenvalues. In these cases the corresponding roots f_j have imaginary parts given either by $\frac{\alpha - \beta}{2}$ or $\frac{\alpha - \beta}{2} - \frac{\pi}{2}$.

In the next section we are going to explore the topology of the above distribution of roots in order to extract the bulk limit ($L \rightarrow \infty$) of the interacting t -vertex model.

V I. T H E R M O D Y N A M I C L I M I T

We shall obtain in this section the free energy $f(\alpha; \beta)$ of the interacting t -vertex model in the bulk limit $L \rightarrow \infty$. The spectral parameter equations (54) or (62) tell us that this interacting model with parameter t ($t = 0; 1; 2; \dots$), on a lattice of size L and density of arrows $\rho = \frac{n}{L}$, is equivalent to a six-vertex model ($t = 0$) on an effective lattice size $L^0 = L - 2nt$ and density $\rho^0 = \frac{n}{L^0} = \frac{n}{L - 2nt}$. This means that in principle we can derive the thermodynamic properties of the interacting t -vertex models by considering the many sectors, with fixed density of arrows, of the six-vertex ($t = 0$) model defined in the helical geometry of Fig. 1b.

Since the relationship among the interacting t -vertex models with distinct values of the parameters t occurs on the eigensectors with distinct numbers n of arrows, we need to evaluate the highest eigenvalue of T_{D-D} on the eigensectors with arbitrary density of arrows $\rho = \frac{n}{L}$. The free energy per site in the bulk limit $f(\alpha; \beta)$ will be obtained from the largest eigenvalue of T_{D-D} . Due to (57) the eigensector containing this eigenvalue will have a density of arrows $\rho = \frac{n}{L}$ that depends

on the particular value of the parameter β , i.e.,

$$f(\beta; \gamma) = \min f(\beta; \gamma); \quad (64)$$

where

$$f = \lim_{n \rightarrow \infty} \frac{1}{n} \sum_{j=1}^n \ln \frac{j}{L} + \ln A; \quad (65)$$

and f_j are the roots of the equations (58) corresponding to the largest eigenvalue of $T_{D,D}$ in the sector with $n = L$ arrows.

The numerical analysis of previous sections (see (61) and (63)) indicates that the roots f_j in (65) correspond to a state with zero momentum and are given by

$$f_j = \frac{\sinh(i \frac{v_j}{2})}{\sinh \frac{v_j}{2}}; \quad v_j = v_{n-j}; \quad j = 1; \dots; n; \quad (66)$$

where v_j are real numbers. Inserting the roots (66) in (62) we verify that both sides of this last equation are unimodular. Using the relations

$$\frac{\sinh(z - iw)}{\sinh(z + iw)} = e^{-i(z;w)}; \quad (67)$$

$$(z;w) = \arctan \frac{2 \tanh z \cot w}{1 - \tanh^2 z \cot^2 w}; \quad (68)$$

we can replace (62) by the equations

$$(L - 2nt) \left(\frac{1}{2} (v_j) + \frac{1}{2} (v_j) \right) = \sum_{j=1}^n I_j + \frac{1}{2} \sum_{j=1}^n (v_1 - v_j); \quad j = 1; \dots; n; \quad (69)$$

where

$$\begin{aligned} \frac{1}{2} (v) &= \left(v; \frac{+}{2} \right); & \frac{1}{2} (v) &= \left(v; \frac{-}{2} \right); \\ \frac{3}{2} (v) &= \left(v; \right); \end{aligned} \quad (70)$$

and I_j are integers or half-odd integers depending if n is odd or even, respectively. Our numerical analysis on small lattices indicates that those integers are given by

$$I_j = j - \frac{n+1}{2}; \quad j = 1; \dots; n; \quad (71)$$

In deriving the equations (62) and (69) it is better to consider separately the cases where the number $n_h =$

$2L - n(2t+1)$ of empty places excluded by the hard-core interactions of the arrows (holes) satisfies $n_h \leq n$ and $n_h < n - \frac{2L}{2t+1}$, or equivalently, $0 \leq n - \frac{L}{t+1}$ or $\frac{L}{t+1} < n - \frac{2L}{2t+1}$. If $\frac{L}{2t+1} < n - \frac{2L}{2t+1}$, we start again our matrix product ansatz (12) by associating now the matrices $A^{(1)}$ and $A^{(2)}$ not to the arrows, as before, but to the empty places excluded by the hard-core sizes of the arrows (holes). The spectral parameter equations we obtain are the same as (62) and (69), except that the number n of variables f_j and f_{v_j} , on the right-hand side of these equations, is replaced by $n_h = 2L - n(2t+1)$.

In order to calculate the free energy (65), as usual, we assume that as $L \rightarrow \infty$ the roots f_{v_j} tend to a uniform distribution on a symmetrical interval of the real axis, $Q - v \leq Q \leq Q + v$. Let us denote by $2(L - 2nt)R(Q, v)dv$ the number of roots f_{v_j} on the interval dv , in the sector with density of roots $\frac{n}{L}$, i.e.,

$$\begin{aligned} \int_{Q-v}^{Q+v} R(Q, v) dv &= \\ \left(\frac{n}{2(L - n(s-1))} = \frac{2(1-t)}{2(1-t)}; \quad 0 \leq \frac{1}{(t+1)}, \right. \\ \left. \frac{2L - (2s-1)n}{2(L - n(s-1))} = \frac{2(2t+1)}{2(1-t)}; \quad \frac{1}{(t+1)} < \frac{2}{(2t+1)} \right); \end{aligned} \quad (72)$$

In terms of this density of roots the function f in (65) is given by

$$f = 2k_B T \ln \int_{Q-v}^{Q+v} R(Q, v) \ln \frac{\sinh(i \frac{+}{2} - v)}{\sinh(i \frac{-}{2} + v)} dv; \quad (73)$$

In order to obtain $R(Q, v)$ we notice from (69) and (71) that for a given value v_j of the variable v_j the integer $I_j + \frac{n+1}{2}$ gives the number of variables v_1 with $1 < j$. Using this fact (69) can be written as [2]

$$\begin{aligned} (L - 2nt) \left(\frac{1}{2} (v) + \frac{1}{2} (v) \right) &= (n+1) \\ + 4(L - 2nt) \int_{Q-v}^{Q+v} R(Q, v^0) dv^0 \\ + 2(L - 2nt) \int_{Q-v}^{Q+v} \frac{1}{2} (v - v^0) R(Q, v^0) dv^0; \end{aligned} \quad (74)$$

Taking the derivative of this last expression, with respect to v , we obtain equations that are conveniently expressed in the trigonometric regime, $\frac{1}{2} = \cos \frac{1}{2}$, by

$$\begin{aligned} R(Q, v) &= \\ \frac{1}{2} \frac{\sin(\frac{+}{2})}{\cosh(2v) \cos(\frac{+}{2})} + \frac{1}{2} \frac{\sin(\frac{-}{2})}{\cosh(2v) \cos(\frac{-}{2})} \\ - \int_{Q-v}^{Q+v} \frac{\sin(2)}{\cosh(2(v - v^0)) \cos(2)} R(Q, v^0) dv^0; \end{aligned} \quad (75)$$

In the hyperbolic regime, where $\cosh v < 1$, it is better to change $\rho \rightarrow i$, $\rho \rightarrow i$, $v \rightarrow iv$, and the equations are

$$\begin{aligned} R(Q, jv) = & \frac{1}{2} \frac{\sinh(\frac{v}{2} + \frac{v}{2})}{\cosh(\frac{v}{2} + \frac{v}{2}) \cos(2v)} + \frac{1}{2} \frac{\sinh(\frac{v}{2} - \frac{v}{2})}{\cosh(\frac{v}{2} - \frac{v}{2}) \cos(2v)} \\ & - \frac{1}{Q} \int_0^Q \frac{\sinh(2v)}{\cosh(2v) \cos(2(v-v^0))} R(Q, jv^0) dv^0; \\ = & \cosh v < 1: \end{aligned} \quad (76)$$

The coupled integrodifferential equations (72) and (75) or (72) and (76) give us, for a given density of roots ρ , the parameter $Q = Q(\rho)$ and the density of roots $R(Q, jv)$. Solving numerically (72) and (75) or (72) and (76) and inserting the result in (73), we obtain $f = f(\rho; t)$. It is important to stress (see (64)) that for given values of the parameters ρ and t the free energy is given by the minimum value of f . In Fig. 7 we show, for $\rho = \frac{1}{3}$ ($\rho = \frac{1}{2}$), $\cosh v = 0.1$, $\cosh v = 1$ the curves f for some values of the parameters t . As we see on this figure the minimum value of f that gives the free energy occurs, for fixed values of the parameters ρ and t , on sectors whose density of arrows depends on the parameters t ($t = 0; 1; 2; \dots$). In the case where $t = 0$ the choice $\rho = 1$ gives us the symmetric six-vertex model on the helical geometry (Fig. 1b). The largest eigenvalue of T_{DD} occurs, in this case, in the sector with density $\rho = 1$. In Fig. 8 we show, for some values of t , the free energy $f = \min f$ as a function of the parameter δ .

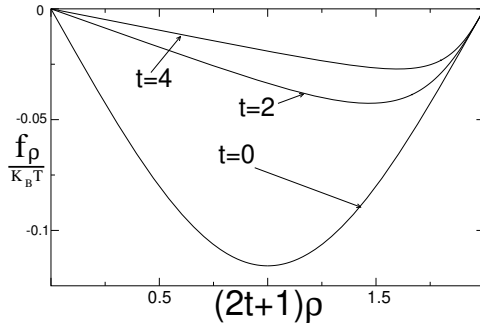


FIG. 7: Functions $f = k_B T$, defined on (65), as a function of ρ , for the interacting vertex model with $t = 0; 2$, and 4. These curves are evaluated for $\cosh v = \frac{1}{2}$, $\cosh v = 0.1$ and $\cosh v = 1$. In this figure the values on the horizontal axis are multiplied by $(2t+1)$ to represent the curves on the same scale. The minimum values of these functions give the free energy.

As we have already mentioned the spectral parameter equations (58) were not analyzed even for the standard symmetric six-vertex model. This case corresponds to the case where $\cosh v = 1$ and $t = 0$ ($s = 1$). Our numerical results (see e.g. Fig. 7) indicate that in this case the parameter Q in (72)–(76) takes the value $Q \rightarrow 1$ and $Q = \infty$ for the trigonometric ($\cosh v < 1$) and the

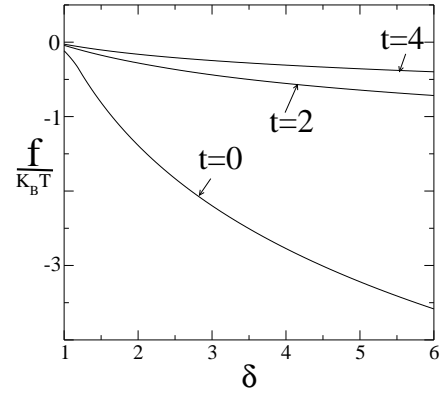


FIG. 8: Free energy, in units of $k_B T$, as a function of δ , for $\rho = 1$ for the interacting vertex models with $t = 0; 2$, and 4. The curves shown are for the anisotropy $\cosh v = \frac{1}{2}$ and parameter $\cosh v = 0.1$.

hyperbolic ($\cosh v < 1$) regimes, respectively. We can use in this case Fourier transforms in order to solve the coupled integrodifferential equations (72) and (75) or (72) and (76). After some straightforward algebra we obtain for $\cosh v = 1$

$$R(Q, jv) = R(1, jv) = \frac{\cosh(\frac{v}{2}) \cos(\frac{v}{2})}{4 \cosh(\frac{2v}{2}) + \cos(\frac{v}{2})}; \quad (77)$$

that gives the free energy

$$\begin{aligned} f = & k_B T \int_0^{\frac{1}{2}} \frac{2 \cosh(\frac{v}{2}) \cos(\frac{v}{2})}{\cosh(\frac{2v}{2}) + \cos(\frac{v}{2})} \\ & \ln \frac{\cosh(2v) \cos(\frac{v}{2})}{\cosh(2v) \cos(\frac{v}{2})} dv; \end{aligned} \quad (78)$$

On the other hand, for $\cosh v < 1$, $\cosh v > 0$, $\cosh v < 1$,

$$\begin{aligned} R(Q, jv) = R(\infty, jv) = & \frac{1}{4} \int_{-\frac{x}{2}}^{\frac{x}{2}} \cosh(\frac{x}{2}) \operatorname{sech}(\frac{x}{2}) e^{ixv} dx \end{aligned}$$

and

$$f = k_B T \left(1 + \sum_{m=1}^{\infty} \frac{(-1)^m}{m} \sinh(2m) \operatorname{sech}(m) e^{-m} \right);$$

In table I we present on the last line the numerical evaluation of the integral (78) for some values of $\cosh v = \cosh v < 1$. In order to compare with the results for finite values of L we also show on this table the results obtained by solving directly the spectral parameter equations (62). The free energy per site in the bulk limit should be independent of the geometry of the lattice. Indeed the results of table I, obtained for the symmetric

six-vertex model in the helical geometry, coincide with those obtained from the row-to-row transfer matrix in the usual geometry (Fig. 1a). It is however interesting to observe that although the final results are the same, the integrand in (78) for the helical case (Fig. 1b) is distinct from the corresponding one in the geometry of Fig. 1a (see Eq. (8.8.19) in [2]).

L	$\gamma = \frac{2}{3}$	$\gamma = \frac{1}{2}$	$\gamma = \frac{1}{3}$
6	0.03512818236	0.06453944019	0.11709717612
10	0.03477636310	0.06406728711	0.11638357858
18	0.03464007645	0.06388499114	0.11610862696
34	0.03459635046	0.06382657413	0.11602059391
66	0.03458384714	0.06380987622	0.11599543821
130	0.03458049496	0.06380539993	0.11598869526
1	0.03457933094	0.06380384561	0.11598635395

TABLE I: Free energy of the six-vertex model ($t = 0$) on the distorted lattice of Fig. 1b for some values of the anisotropy $\gamma = \cos \theta$ and lattice sizes L . The values are obtained by solving (62) with $\gamma = 0.1$ and using (61) and (65) with $\gamma = 1$. The last line gives the bulk limit obtained by solving (78).

VII. CONFORMAL INVARIANCE AND OPERATOR CONTENT

In this section, by exploring the conformal invariance of the infinite system, we shall obtain the critical behavior of the massless phases of the interacting six-vertex models introduced on this paper. The results of the last section tell us that for $\gamma < 1$ the eigensector of T_D presenting the largest eigenvalue, changes continuously with the value of the interacting parameter γ . This implies that for $\gamma < 1$ the introduced interacting models with arbitrary values of $t = 0; 1; 2; \dots$ are on a critical phase, as we change continuously the parameter γ in the bulk limit ($L \rightarrow \infty$). This behavior for the case $t = 0$ ($s = 1$) is expected since, as we discussed in earlier sections, the interacting model recovers the six-vertex model. In this case the interacting parameter γ plays the role of a chemical potential (or electric field) controlling the density of arrows. The critical behavior of this six-vertex model follows from that of the XXZ chain in the presence of an external magnetic field [16]. The region where $\gamma > 1$ (ferroelectric region) is non-critical for any value of t and s . The largest eigenvalue of T_D belongs to the sector with no arrows ($\gamma = 0$), for $\gamma < 1$, or to the sector with the largest possible density of arrows ($\gamma = \frac{2}{2t+1}$) for $\gamma > 1$.

The conformal anomaly and anomalous dimensions (related to the critical exponents) of the underlying conformal field theory governing the critical fluctuations on the critical phase of our models are going to be calculated from the finite-size corrections of the eigenvalues of the transfer matrix T_D , or the related Hamiltonian

$H = -\ln(T_D)$. The leading behavior, as $L \rightarrow \infty$, of the smallest eigenvalue $F_0(L)$ of H (ground-state energy) [19]:

$$F_0(L) = F_0(\infty) - \frac{v_s c}{6L} + o(L^{-1}) \quad (79)$$

gives the conformal anomaly c and the sound velocity v_s . Moreover, to each primary operator with dimensions x , in the operator algebra of the critical system, there exists an infinite tower of eigenstates of $H = -\ln(T_D)$, whose eigenvalues $F_{m,j}^{(L)}$ behaves asymptotically as [20]

$$F_{m,j}^{(L)}(L) = F_0(L) + \frac{2}{L} (x + m + m^0) + o(L^{-1}); \quad (80)$$

with $m, m^0 = 0; 1; 2; \dots$.

Before considering our model with general values of t ($t = 0; 1; 2; \dots$) and s , let us consider the special case where $t = 0$ and $s = 1$. In this case we recover the standard symmetric six-vertex model in the absence of electric fields, but for the helical geometry of Fig. 1b. Similarly, as in the standard geometry of Fig. 1a [21], our numerical and analytical analysis indicate that the model is critical for $1 < \gamma < 1$, and massive for $\gamma > 1$. In agreement with earlier studies of the six-vertex on the standard geometry, and of the XXZ quantum chain [14], the critical fluctuations in the region $1 < \gamma = \cos \theta < 1$, are governed by a conformal field theory with central charge $c = 1$ and anomalous dimensions given by

$$x_{n,m} = n^2 x_p + \frac{m^2}{4x_p}; \quad n, m = 0; 1; 2; \quad (81)$$

where

$$x_p = \frac{1}{2}; \quad (82)$$

Our numerical and analytical analyses show that distinctly from the row-to-row transfer matrices in the standard geometry where the sound velocity is unity [17, 18, 20], in the helical geometry one has $v_s = v_s(\gamma) \neq 1$. The sound velocity from (79) can be calculated from the bulk limit of the finite-size sequence

$$v_s^{(L)} = [F_0(L) - F_0(\infty)] \frac{6L}{c}; \quad (83)$$

For $\gamma = 0$ ($\gamma = \frac{2}{3}$) we can compute analytically these finite-size corrections and obtain

$$v_s = \frac{1}{2} \tan \frac{\theta}{2}; \quad (84)$$

For $\gamma \neq 0$ our calculations were done numerically and we do not have an analytical form for v_s . In table II we

show some of the estimates $v_s(L)$ given by (83) obtained for some values of $t = 0.1$. In order to illustrate our numerical evaluation of the dimensions (81) we show in table III, for $t = 0.1$ and some values of Δ , the finite-size estimates for x_p , together with the expected results (82). These estimates are obtained by using in (80) the largest eigenvalues of $T_{D,D}$ in the sectors with $n = L$ and $n = L - 1$ arrows.

L	$\Delta = \frac{2}{3}$	$\Delta = \frac{1}{2}$	$\Delta = \frac{1}{3}$
6	0.03773624455	0.05057575759	0.07637450614
10	0.03763037006	0.05031361905	0.07586431519
18	0.03758898261	0.05021239628	0.07566185294
34	0.03757566153	0.05017995742	0.07559488486
66	0.03757184873	0.05017068491	0.07557509072
130	0.03757082640	0.05016819918	0.07556960190

TABLE II: Finite-size estimators $v_s(L)$ for the sound velocity of the six-vertex model ($t = 0$) on the distorted lattice of Fig. 1b. The values are given for some values of the anisotropy $\Delta = \cos \theta$ and lattice sizes L .

L	$\Delta = \frac{2}{3}$	$\Delta = \frac{1}{2}$	$\Delta = \frac{1}{3}$
6	0.16676687232	0.24712196038	0.32156619180
10	0.16669813477	0.24895867881	0.32848712047
18	0.16667118823	0.24967533316	0.33163455071
34	0.16666377768	0.24990588089	0.33279409868
66	0.16666111003	0.24997186077	0.33308163424
130	0.16666077565	0.24998955436	0.33328029440
x_p	0.1666..	0.25	0.3333..

TABLE III: Finite-size estimators for the critical exponent x_p of the six-vertex model on the distorted lattice ($t = 0$) of Fig. 1b. The values are given for some values of the anisotropy $\Delta = \cos \theta$ and lattice sizes L . These estimators are obtained by solving (62).

Let us consider the general case where $t = 0; 1/2; \dots$ and $\Delta > 0$. In this case we have a massless phase for $\Delta < 1$. For a given value of Δ the density of arrows ρ , in the bulk limit, is obtained by the condition $\frac{df}{d\rho} = 0$, where f is given by (73). As we change Δ , from zero to infinity, ρ increases from 0 to $\frac{2}{2t+1}$. Our numerical analysis indicates that the underlying conformal field theory, as in the case $t = 0$ and $\Delta = 1$, has also a central charge $c = 1$ and the Coulomb gas type of conformal dimensions given in (81), but with a value of x_p that depends on Δ , and t . The parameter x_p , that can be estimated from the finite-size corrections of the smallest eigenvalues of $H = \ln(T_{D,D})$, can be calculated analytically. This is done by applying to our relations (72)–(76) of last section, the method used in [22] for the XXZ in a magnetic field. We obtain

$$x_p = \frac{1}{4} (1 - t)^2 - \frac{1}{2} (Q j^p) \quad (85)$$

where, for $\Delta = \cos \theta$,

$$(Q j^p) = 1 - \frac{1}{Q} \sum_{\nu} \frac{\sin(2\theta - \nu)}{\cosh(2(\nu - \nu^0)) \cos(2\theta)} dv^0; \quad (86)$$

and, for $\Delta = \cosh \theta < 1$,

$$(Q j^p) = 1 - \frac{1}{Q} \sum_{\nu} \frac{\sinh(2\theta - \nu)}{\cosh(2\theta) \cos(2(\nu - \nu^0))} dv^0; \quad (87)$$

For a given density of arrows the parameter $Q = Q(\Delta)$ is obtained by solving the coupled integral equations (72) and (75) for $\Delta < 1$, and (72) and (76) for $\Delta = \cosh \theta < 1$. Similar integral equations happen for the XXZ chain with hard-core exclusion effects [23].

At $t = 0$ Eq. (86) gives $(Q j^p) = 1$, and from (87) we obtain the curve

$$x_p = \frac{1}{4(1 - t)^2}; \quad \Delta = 0: \quad (88)$$

For fixed values of t ; and Δ (or θ) the interacting parameter will fix the density of arrows as well as the parameters $Q = Q(\Delta)$ appearing in (72), (75) (or (76)) and (85)–(87). In Fig. 9 we show the curves of x_p as a function of Δ at $t = \frac{1}{2}$ and for some fixed values of t . In Fig. 10 and Fig. 11 the values of x_p as a function of Δ are shown for the interacting model with parameter $t = 2$. The curves of Fig. 10 and Fig. 11 are for the regimes $\Delta > 1$ and $\Delta < 1$, respectively.

As we see in Fig. 10 and Fig. 11 the curves have a common intercept $x_p = 1/4$ at $\Delta = 0$ and $x_p = 25/4 = 6.25$ at $\Delta = 2/5 = 0.4$. In fact our numerical results, for arbitrary values of t and Δ , show that at low density ($\rho \rightarrow 0$) and high density of arrows ($\rho \rightarrow \frac{2}{2t+1}$) the anomalous dimension x_p take the values $x_p = 1/4$ and $x_p = \frac{(2t+1)^2}{4}$, respectively. This happens because at those extreme limits either the density of arrows or the density of holes is low and the anisotropy Δ , that is only important for the arrows (holes) at the closest positions, plays no role.

We also see in Fig. 11 the appearance of a peak ($x_p = 6^2/4 = 9$) at the density $\rho = \frac{1}{3}$, that is independent of the anisotropy Δ . For general values of t and $\Delta < 1$ this peak occurs at the "half-filled" density $\rho = \frac{1}{t+1}$, for any $\Delta < 1$. This happens because, for $\Delta < 1$, the system at this "half-filling" has a mass gap. An infinitesimal change of Δ (induced by a change of t) destroys this mass gap. Since around this density the main effect is the disappearance of the gap, the critical exponent x_p does not depend on the Δ value. A similar effect is also expected in the region $\Delta < 1$ of the XXZ or six-vertex model on the presence of an external magnetic field.

V III. CONCLUSIONS

We have introduced in this paper a special family of exact solvable interacting ν -vertex models. Besides the

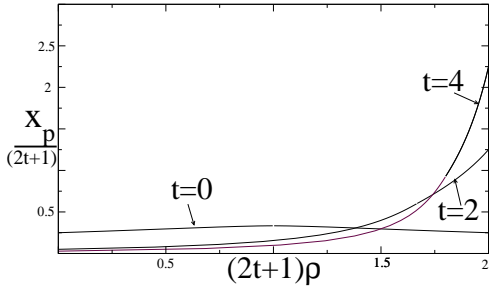


FIG. 9: The critical exponent x_p , as a function of ρ , for the interacting vertex models with $\gamma = \frac{\pi}{2}$ and interacting parameter $t = 0; 2$ and 4 . In the figure the horizontal and (vertical) axis are multiplied (divided) by $2t + 1$ in order to represent the curves on the same scale.

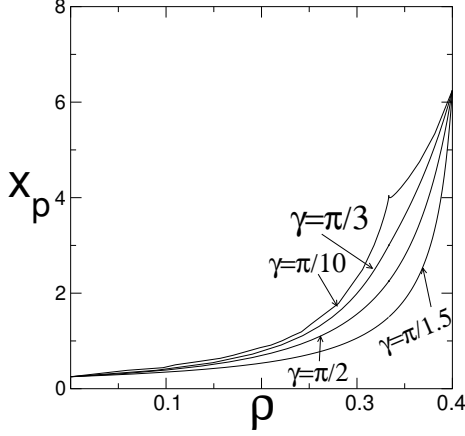


FIG. 10: The critical exponent x_p , as a function of ρ , for the vertex model with interacting parameter $t = 2$ and some values of the anisotropy $\gamma = \cos^{-1} \rho$.

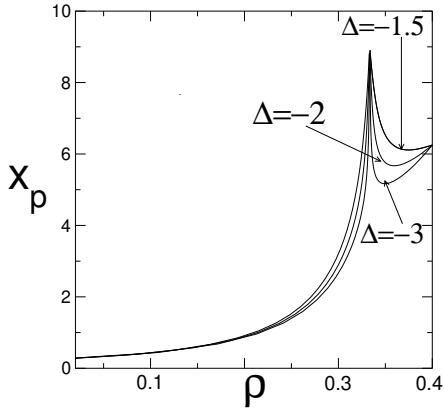


FIG. 11: The critical exponent x_p , as a function of ρ , for the vertex model with interacting parameter $t = 2$ and some values of the anisotropy $\Delta < -1$.

usual nearest-neighbor interactions imposed by the lattice connectivity, such models also present hard-core interactions along one of the diagonals of the lattice. The range of the additional interactions depend on a fixed parameter t ($t = 1; 2; \dots$). These vertex models can also be interpreted as if the arrows entering in the vertex configurations have an effective hard-core size $s = 2t + 1$. This interpretation allows us to identify the extension of these models to the case $t = 0$ ($s = 1$) as the standard six-vertex model. In this sense, although our interacting models have only one vertex, they are generalizations of the standard six-vertex model.

Although the exact solution of the transfer matrix are usually obtained through the Bethe ansatz, we have derived the solution of these models by using the matrix product ansatz introduced in [6], to perform the exact diagonalization of quantum chains. This first application indicates that this ansatz is also suitable for transfer matrix calculations.

Due to the extra interactions along the diagonals of the lattice, the solution of these models was simplified by considering the diagonal-to-diagonal transfer matrix. A numerical analysis of the spectral parameter equations for small lattices enabled the calculation of the free energy of the models in the bulk limit. This calculation was done on a symmetric version of the model that recovers for $t = 0$ the symmetric six-vertex model. Our results show that the models, for any value of t ($t = 0; 1; 2; \dots$), exhibit a massless phase for arbitrary values of the anisotropy given by (59). Exploring the consequences of the conformal invariance of the infinite system we also calculate, on the massless phase, the conformal anomaly, the sound velocity and the operator content of the underlying field theory governing the long-distance critical fluctuations. Underlying these models there is a $c = 1$ conformal field theory whose operators have a Coulomb gas type of anomalous dimensions $x_{n,m}$ (see (81)). The compactification ratio defining these dimensions varies continuously with the free parameters of the model. Our analytical and numerical calculations show that the effect of the interacting parameter t is to increase the critical exponents as t increases, while the extra interaction energy, related to the parameter ρ , plays the role of a chemical potential controlling the number of arrows on the ground state eigenfunction.

Acknowledgments

We thank V. Rittenberg for helping us to find the representation (55) and L. A. Ferreira for fruitful discussions and a careful reading of the manuscript. This work has been partially supported by the Brazilian agencies FAPESP and CNPq.

- chanics (New York: Academic) (1982).
- [3] M. Gaudin, *La Fonction d'Onde de Bethe* (Paris: Masson) (1983).
- [4] R. F. Wang et al, *Nature* 439, 303 (2006); S. T. Bramwell, *Nature* 439, 273 (2006).
- [5] H. A. Bethe, *Z. Phys.* 71, 205 (1931).
- [6] F. C. Alcaraz and M. J. Lazo, *J. Phys. A* 37, L1 (2004); *J. Phys. A* 37, 4149 (2004); *Braz. J. Phys.* 33, 533 (2003).
- [7] This notation is chosen in order to compare these interacting vertex models with the standard six-vertex model.
- [8] R. Z. Bariev, *Mat. Fiz.* 49, 261 (1981).
- [9] T. T. Truong and K. D. Schotte, *Nucl. Phys. B* 20 [FS8], 77 (1983).
- [10] This last case only is allowed in the case of the six-vertex model where $t = 0$ and $s = 1$.
- [11] O. Golinelli and K. Mallick [arXiv:cond-mat/0604338](https://arxiv.org/abs/cond-mat/0604338).
- [12] F. C. Alcaraz and R. Z. Bariev, *Phys. Rev. E* 60, 79 (1999).
- [13] The phase $e^{i2\pi t}$ in (54) could be obtained by considering a six-vertex model on the geometry of Fig. 1b, but with a seam with distinct vertex fugacities along the vertical direction.
- [14] F. C. Alcaraz, M. N. Barber, and M. T. Batchelor, *Phys. Rev. Lett.* 58, 771 (1987); *Ann. Phys. (N.Y.)* 182, 280 (1988).
- [15] H. Y. Huang, F. Y. Wu, H. Kunz and D. Kim, *Physica A* 228, 1 (1996).
- [16] J. D. Johnson and B. M. McCoy, *Phys. Rev. A* 6, 1613 (1972); M. Takahashi, *Prog. Theor. Phys.* 50, 1519 (1973).
- [17] In the XXZ chain with anisotropy $\Delta = \cos \theta$ the sound velocity is $v_s = \frac{\sin \theta}{2}$.
- [18] M. T. Batchelor, M. N. Barber and P. A. Pearce, *J. Stat. Phys.* 49, 1117 (1987).
- [19] H. Blote, J. L. Cardy and M. Nightingale, *Phys. Rev. Lett.* 56, 742 (1986); I. A. A. Eck, *Phys. Rev. Lett.* 56, 186 (1986).
- [20] See, e.g., J. L. Cardy in *Phase Transitions and Critical Phenomena*, vol. 11, edited by C. Domb and J. L. Lebowitz (Academic, New York, 1986); J. L. Cardy, *Nucl. Phys. B* 270, 186 (1986).
- [21] N. M. Bogoliubov, A. G. Izergin and V. Korepin, *Nucl. Phys. B* 275, 687 (1986).
- [22] F. W. Obyedkov, H. P. Eckle and T. T. Truong, *J. Phys. A* 22, 4027 (1989).
- [23] F. C. Alcaraz and R. Z. Bariev in *Series on Advances in Statistical Mechanics*, vol. 14, edited by M. T. Batchelor and L. T. Wille (World Scientific, Singapore, 1999).